Research Square

Preprints are preliminary reports that have not undergone peer review.
They should not be considered conclusive, used to inform clinical practice,
or referenced by the media as validated information.

Future Tibetan Plateau Winter Warming Increases the Frequency of Negative PNA Events

Fiona Richer

fiona.richer@uib.no

Universitetet i Bergen https://orcid.org/0009-0009-5544-2811

Lea Svendsen

UIB: Universitetet i Bergen

Ingo Bethke

UIB: Universitetet i Bergen

Fei Li

UIB: Universitetet i Bergen

Research Article

Keywords:

Posted Date: August 24th, 2026

DOI: https://doi.org/10.21203/rs.3.rs-10636963/v1

License: This work is licensed under a Creative Commons Attribution 4.0 International License.
Read Full License

Future Tibetan Plateau Winter Warming increases the Frequency of Negative PNA Events

Fiona Richer[1,2*], Lea Svendsen[1,2], Ingo Bethke[1,2], Fei Li[1,2]

[1]Geophysical Institute, University of Bergen, Bergen, Norway.
[2]Bjerknes Centre for Climate Research, Bergen, Norway.

*Corresponding author(s). E-mail(s): fiona.richer@uib.no;

Abstract

Previous studies have identified a teleconnection between Tibetan Plateau (TP) winter snowfall anomalies and the Pacific–North American (PNA) pattern, based primarily on observations under present-day climate conditions. Whether this relationship persists under future TP warming remains uncertain. Here we isolate the atmospheric response to an idealized TP warming perturbation of 4 °C, comparable to the projected end-of-century signal, using atmosphere-only general circulation model experiments with fixed sea surface temperatures and sea ice. Enhanced heating over the TP generates upper-level divergence and an anticyclonic anomaly that weakens the subtropical jet and displaces the jet exit westward over the central North Pacific. There, wave activity generated over the plateau is released and propagates downstream, producing circulation anomalies over North America that closely resemble the observed negative PNA pattern. The PNA distribution from a Warm TP retains the same distribution and variance but is displaced toward more negative values, increasing the frequency of negative PNA months from 16% to 26%. These findings suggest that continued TP warming may systematically alter the winter atmospheric circulation over the North Pacific and North America increasing the likelihood of negative PNA events.

1 Introduction

As the world's highest and largest plateau, the Tibetan Plateau's (TP) thermal and mechanical forcing imposes a significant influence on both the regional and global climate (Zhou et al. 2023). Over the past few decades, the TP has warmed at an accelerated rate, more than 1.5 times the global average (Hu et al. 2024). The warming stems from anthropogenic forcing, which drives the reduction of glaciers and snow cover, and is therefore enhanced by the snow-albedo feedback (Hu et al. 2023). Since 1985, the TP has lost over one-fifth of its glacier mass and is projected to lose up to two-thirds of its present mass by 2100 (United Nations Environment Programme 2022). Furthermore, winter (DJF) temperatures over the TP are projected to increase by up to 3.3 °C (6.0 °C) under the SSP2-4.5 (SSP5-8.5) scenarios by the end of the century (Hu et al. 2023; Meng et al. 2023; Hu et al. 2024). These projections, however, remain uncertain, in part due to a persistent cold bias over the TP that is most pronounced during the freezing season, meaning the warming could be even larger (Zhou et al. 2023). This bias is largely linked to difficulties in representing snow, cloud cover, and the complex terrain. If models underestimate TP warming, they may also underestimate its dynamical impact on global atmospheric circulation.

The elevated thermal forcing over the TP plays an important role in altering atmospheric circulation. In summer, TP warming induces dry and warm conditions upstream, extending to the North Atlantic, and wet conditions in the Sahel region (Lu et al. 2018). The thermal forcing also plays a key role in the Asian summer monsoon (Huang et al. 2023). In winter, anomalous TP warming creates favorable conditions for the formation of persistent freezing rain over central and southeastern China (Bao et al. 2010).TP snow anomalies in winter have been found to influence North American climate through the Pacific–North American (PNA) pattern (Wang et al. 2020; Liu et al. 2017; Lin and Wu 2012; Wu et al. 2011; Liu et al. 2020). The PNA is the second leading mode of Northern Hemisphere winter variability and a

dominant driver of North American temperature and precipitation anomalies.

The TP-PNA teleconnection was first introduced by Lin and Wu (2011), discovering that positive (negative) autumn TP snow cover anomalies can induce a positive (negative) PNA-like pattern in winter. Lin and Wu (2011) propose a mechanism in which increased snow cover induces negative geopotential height anomalies, which impose an anomalous vorticity perturbation near the East Asian westerly jet core. The jet carries these perturbations eastward, crossing the North Pacific Ocean to form a wave train-like pattern, resulting in a PNA-like surface temperature response over North America. However, more recent studies have also found this relationship to be weakening in the past decade in conjunction with TP warming and a weakened cooling in winter (Qian et al. 2019). Moreover, the signal is competing with stronger future sea surface temperature (SST) anomalies in the tropical central Pacific, which impose their own impact on the North American climate (Wang et al. 2020).

Despite the findings mentioned above, the role of the primary atmospheric pathway of the TP-PNA teleconnection is still unclear. In particular, coupling to a dynamic ocean introduces additional internal variability and nonlinearity, complicating efforts to isolate the causal atmospheric response to thermal forcing and to assess its dependence on the background circulation state. Furthermore, many previous studies rely on observations or simulations under present-day conditions, limiting the ability to establish a direct causal link between TP warming and the PNA response. Additionally, the role of snowfall anomalies may become less relevant in the future as background temperatures increase and snowfall over the TP declines.

This study reevaluates the TP–North American teleconnection with an idealized future TP warming perturbation using a deliberately controlled atmospheric

framework. Isolating the atmospheric response to TP warming, therefore, provides important insight into the potential influence of future TP thermal forcing on the variability and predictability of the PNA.

2 Data and Methods

2.1 Model Experiments

To isolate the effects of TP warming on atmospheric circulation and remote climate, Atmospheric General Circulation Model (AGCM) experiments are performed. A non-coupled experiment provides a more controlled framework to isolate the dynamical atmospheric responses from the TP. Each experiment is run as 100-year time-slice simulations, using the medium-resolution configuration of the Norwegian Earth System Model version 2 (NorESM2-MM) in an atmosphere-land only configuration (Seland et al. 2020). This configuration utilizes a horizontal resolution of $\sim 1^\circ$ and 32 vertical levels on hybrid coordinates. Sea surface conditions, including sea ice, have a fixed seasonal variation repeated every year and are prescribed throughout the entirety of the simulation. SSTs follows the climatology from 1995–2005. Boundary conditions and external forcings are climatological for the year 2000, consistent with the CMIP6 PAMIP experiment protocol for pdSST-pdSIC (Smith et al. 2019). Because SST, sea ice and external forcings follow a repeating annual cycle, all variability in the response is internally generated, and the length of the simulations provides strong statistical confidence in the circulation response.

To minimize the influence of already realized anthropogenic warming, a composite of monthly sea-ice maxima based on NOAA satellite observations (Meier et al. 2024) from 1982 to 2024 is prescribed. The dataset consists of daily observations gridded at 0.25° x 0.25° resolution, which are first averaged into monthly means. For each calendar month, the maximum value at each grid point is selected to construct the final ice concentration. To ensure compatibility with the Community Atmosphere Model (CAM), the sea-ice data are regridded to a $1.25^\circ \times 0.9^\circ$ longitude-latitude horizontal resolution and temporally adjusted to better represent conditions on the 15th day of each month. The base simulation is named CONTROL.

To force warming over the TP an additional fixed downward longwave flux of $30\,\mathrm{W\,m^{-2}}$ is imposed over the TP region resulting in a surface warming of $4\,^{\circ}\mathrm{C}$ in boreal winter defined as December-February (DJF) (Figure 1b). This approach has previously been successfully applied to study coupled model responses to reduced Arctic sea ice cover in Deser et al. (2015). In that study, the additional longwave radiative flux was prescribed only to the sea-ice model, and only where and when sea ice was present, as a nudging technique to obtain a target Arctic sea-ice state. Thus, the imposed flux was mainly a technical device to produce sea-ice loss. In the present experiment, however, the added downward longwave flux is applied directly over land and serves as the primary forcing used to warm the TP surface. The forcing magnitude was selected following sensitivity experiments and scaling based on the Stefan–Boltzmann relationship, such that the resulting surface warming approximately matches the end-of-century TP warming signal shown in Figure 1a. This additional downward flux is applied above 2500m elevation over the region 25°–45°N and 69°–110°E in Figure 1b. Between 1500 and 2500m elevation, the forcing is tapered linearly. This experiment is henceforth referred to as WTP. The climate response to the imposed TP warming is diagnosed from differences between the 100-year means of WTP and CONTROL. Statistical significance is assessed using a two-tailed Student's t-test at the 95% confidence level. Tests are performed using seasonal (DJF) means, with each winter treated as an independent realization.

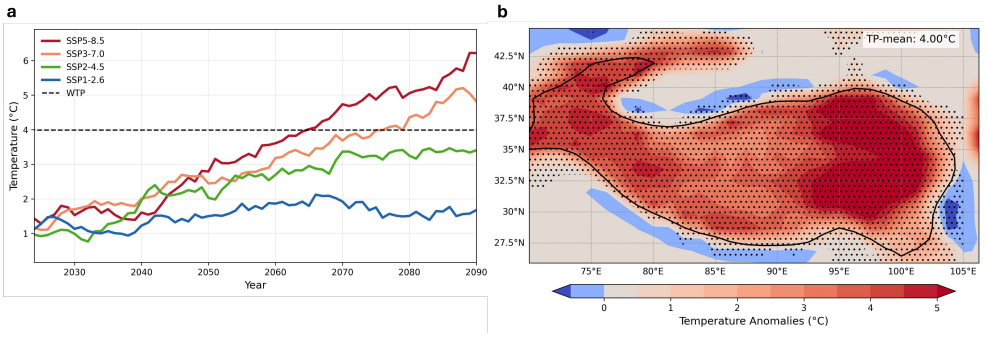


Fig. 1: (a) DJF surface air temperature anomalies over the TP (25–60°N, 69–110°E) from NorESM SSP scenarios relative to the 1995–2014 climatology. Colored lines show 10-year running mean anomalies for SSP1-2.6 (blue), SSP2-4.5 (green), SSP3-7.0 (orange), and SSP5-8.5 (red). The horizontal dashed line indicates the imposed TP warming in the WTP experiment. (b) Mean winter surface air temperature anomalies (°C) over the TP in the WTP experiment relative to the CONTROL. The black contour denotes the 2500m elevation boundary used to define the TP region, within which the TP-mean warming is calculated. Stippling indicates statistical significance at the 95% confidence level.

2.2 Wave Flux

Stationary wave propagation is obtained using the plumb wave activity calculated from monthly mean 200-hPa geopotential height following Plumb (1985). The diagnostic is based on linearized quasi-geostrophic theory on a zonally varying basic state and illustrates the direction and magnitude of stationary Rossby wave propagation.

2.3 PNA Index

The PNA index is calculated using a regional box definition from the Climate Prediction Center (NOAA Climate Prediction Center 2005).

$$\begin{aligned} \mathrm{PNA} = \big[\, & Z^*(15\text{–}25^\circ\mathrm{N},\ 180\text{–}140^\circ\mathrm{W}) - Z^*(40\text{–}50^\circ\mathrm{N},\ 180\text{–}140^\circ\mathrm{W}) \\ & + Z^*(45\text{–}60^\circ\mathrm{N},\ 125\text{–}105^\circ\mathrm{W}) - Z^*(25\text{–}35^\circ\mathrm{N},\ 90\text{–}70^\circ\mathrm{W}) \big] \end{aligned} \tag{1}$$

where Z^* denotes the wintertime mean 500-hPa geopotential height anomaly and the parenthetical terms denote area averages over the four regional domains.

To compare the simulated circulation response with observations, ERA5 reanalysis data are used to construct a negative PNA composite. All winter months between 1950–2025 with a PNA index below -1 one standard deviation are selected, and defined as negative-PNA months. Anomalies in monthly mean 500-hPa geopotential height, precipitation and near-surface air temperature from negative-PNA months are computed relative to the 1950–2000 climatology, consistent with the NOAA NCEI index definition. This composite is used to characterize the observed circulation and hydroclimate response associated with negative PNA phases and will be referred to as OBS PNA−.

The PNA index from each experiment is calculated then standardized using the mean and standard deviation of the CONTROL simulation. The probability of a negative-PNA month, P(PNA < -1), is estimated in each experiment as the fraction of occurrences over the 300 simulated DJF months. Uncertainty is quantified by bootstrap resampling: each sample is resampled with replacement 10,000 times, P(PNA < -1) is recomputed for each resample, and the 2.5th and 97.5th percentiles of the resulting distribution define the 95% confidence interval.

3 Results

3.1 PNA Response

Figure 2a displays the atmospheric response over North America for the WTP experiment (top row) and the OBS PNA− (bottom row). The simulated anomalies exhibit strong spatial agreement with observed negative PNA patterns, with pattern correlations of 0.90 for geopotential height, 0.84 for temperature, and 0.56 for precipitation over the displayed domain. The response is characterized by warm anomalies over Alaska and eastern North America, cooler conditions over the western United States, and reduced precipitation along the Canadian west coast.

A comparison of the distribution of the PNA indices is displayed in Figure 2b. The WTP mean is displaced toward a more negative state, at -0.37 compared to the CONTROL at 0. The width of the distribution, however, remains relatively unchanged, indicating that a WTP does not alter the variance of PNA events, but instead shifts the background state. This displacement corresponds to a higher frequency of negative-PNA months, where P(PNA <-1) increases from 0.16 in CONTROL to 0.26 in WTP, which represents a relative increase of 64% (Figure 2c). On the other hand, positive PNA events, where P(PNA <-1), decrease from 0.15 in CONTROL to 0.10 in WTP.

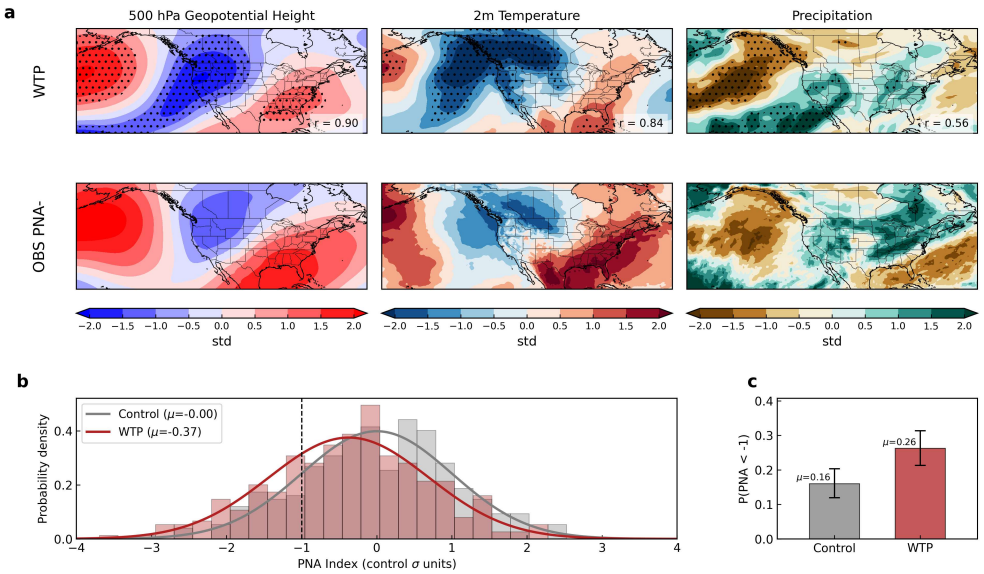


Fig. 2: Overview of the PNA pattern in both the WTP and CONTROL experiment. (a) DJF standardized anomalies of 500 hPa geopotential height (Z500), 2 m temperature (TREFHT), and precipitation (PRECT) for WTP-CONTROL (top row), and for the OBS PNA− (ERA5, 1950–2025; bottom row). Stippling in the WTP row indicates grid points where the WTP–CONTROL difference is statistically significant at the 95% confidence level. Pattern correlation coefficients (r) between the WTP and OBS PNA− fields for each variable are given in the lower-right corner of each panel. (b) Distribution of the DJF standardized PNA for the CONTROL (gray) and WTP (red) experiments with Gaussian fits overlaid. The dashed vertical line marks the threshold used to define a negative-PNA event (PNA <-1). (c) Probability of PNA <-1 in the CONTROL and WTP experiments, with error bars showing 95% bootstrap confidence intervals (n = 10,000 resamples).

3.2 Mechanisms Behind the PNA Emergence

In order to better understand and quantify this teleconnection it is crucial to outline the driving mechanism. Enhanced surface heating over the Tibetan Plateau of 1 °C or greater extends upward to approximately 400 hPa where it then weakens further toward the tropopause (Figure 3a). The heat anomaly exhibits a clear eastward tilt with height, reflecting advection by the mean westerly flow. The associated ascent over the plateau induces strong upper-level divergence. This divergent outflow generates

negative potential vorticity (PV) anomalies of −0.10 to −0.22 PVU in the upper troposphere (Figure 3b). The associated upper-level divergence acts as a Rossby wave source, initiating downstream wave propagation into the North Pacific. The upper-level negative anomaly is accompanied by positive PV anomalies below, consistent with the vertical dipole expected from mid-tropospheric diabatic heating.

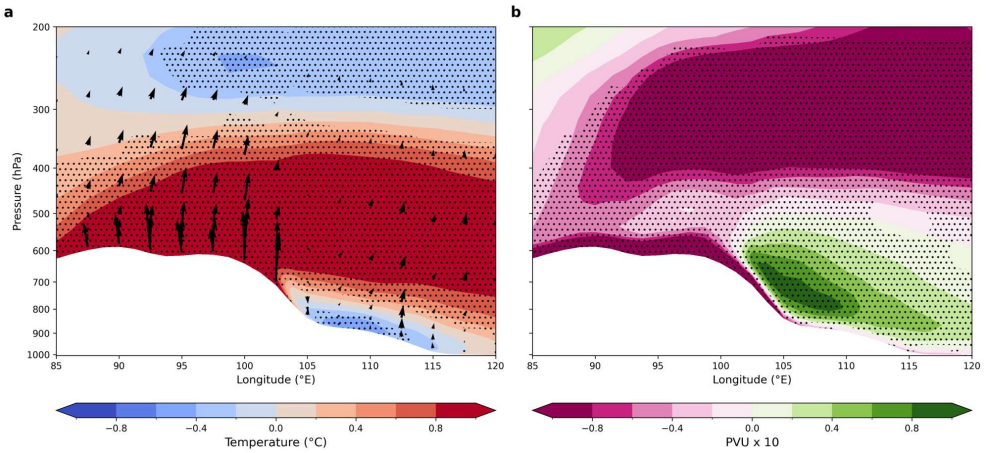


Fig. 3: Zonal cross-section (30–40°N) of DJF WTP−CONTROL anomalies in (a) temperature (°C) and (b) potential vorticity (PVU ; $10^{-6}\mathrm{K\,m^2\,kg^{-1}\,s^{-1}}$). Arrows indicate circulation anomalies, with vertical velocity (Pa/s) scaled by −200 relative the horizontal velocity (m/s). Stippling denotes significance at the 95% confidence level.

The upper-level divergence also drives an anticyclonic circulation anomaly, which weakens and retracts the subtropical jet (Figure 4a). Zonal wind speeds at 200 hPa are reduced by approximately 2–3 $\mathrm{m\,s^{-1}}$ downstream of the TP, with the strongest weakening occurring over the central North Pacific. The jet exit, defined as the longitude at which the core 200 hPa wind speed falls below 55$\mathrm{m\,s^{-1}}$, is positioned at 179°E, which is 4°W of the CONTROL jet exit. This shift is critical, as it marks the region where the mean flow decelerates and is no longer zonally confined. This is evident from localized regions of enhanced zonal wind speeds (2–3 $\mathrm{m\,s^{-1}}$) to the north

and south of the CONTROL jet downstream of the jet exit, indicating the meridional dispersion of the flow.

The findings are consistent with the wave activity flux pattern in Figure 4b. Wave activity is initially generated over the divergence zone near the TP. The strongest wave activity fluxes emerge over the North Pacific in the vicinity of the WTP jet exit and propagate downstream across North America. The strongest wave activity flux (WAF) magnitudes are collocated with maximum geopotential height anomalies, comprising the features of a traditional negative PNA-like circulation pattern.

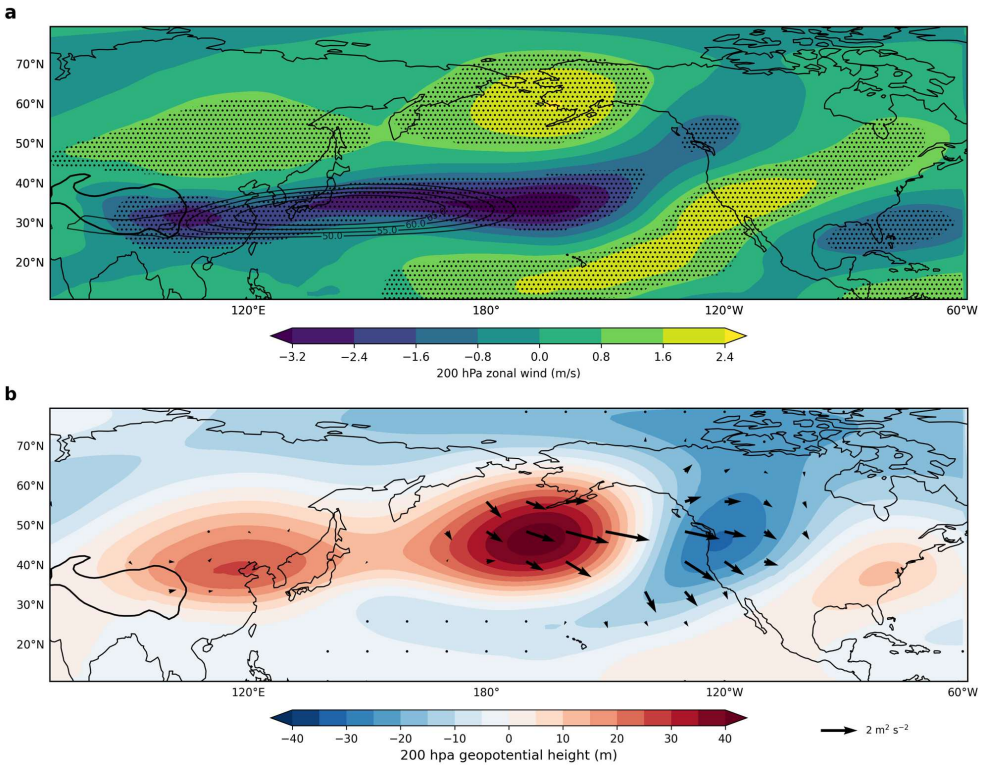


Fig. 4: DJF WTP−CONTROL anomalies for (a) Winter 200 hPa zonal wind anomalies ($\mathrm{m\,s^{-1}}$) where the black contours indicate maximum zonal wind speeds in the CONTROL. (b) Color shading represents 200 hPa geopotential height anomalies. Black vectors represent the stationary wave activity flux ($\mathrm{m^2\,s^{-2}}$) where wave flux anomalies are statistically significant at the 95% confidence level. The black contour outlines the 2500m elevation of the Tibetan Plateau.

4 Discussion and Conclusion

This study details how wintertime warming over the TP modifies the frequency of the PNA emergence through purely atmospheric processes. Using idealized 100-year atmospheric experiments, we isolate the response of the TP and directly compare the resulting circulation anomalies with a composite of negative PNA events from ERA5. We show that a thermally induced perturbation over the TP ($30\,\mathrm{W\,m^{-2}}$), acting alone and within a realistic warming range, is sufficient to shift the mean atmospheric state toward a more negative PNA phase. The PNA distribution is displaced by -0.37 with no detectable change in its variance, raising the frequency of negative PNA months from 16% to 26%. Therefore enhanced TP warming may increase the likelihood of negative PNA conditions in the future.

The proposed mechanism of this teleconnection is summarized in Figure 5. Enhanced surface heating over the TP strengthens ascent and induces upper-level divergence, generating negative potential vorticity anomalies east of the plateau that act as a localized Rossby wave source. During the winter months, the subtropical jet is positioned sufficiently southward to intersect the TP, enabling interaction between the forcing and the mean flow. The associated upper-level anticyclonic anomaly weakens the jet, and retracts it westward, displacing the jet exit over the central North Pacific. Wave activity generated over the plateau is confined zonally along the jet and released near the exit, favoring the development of a negative PNA-like pattern over North America.

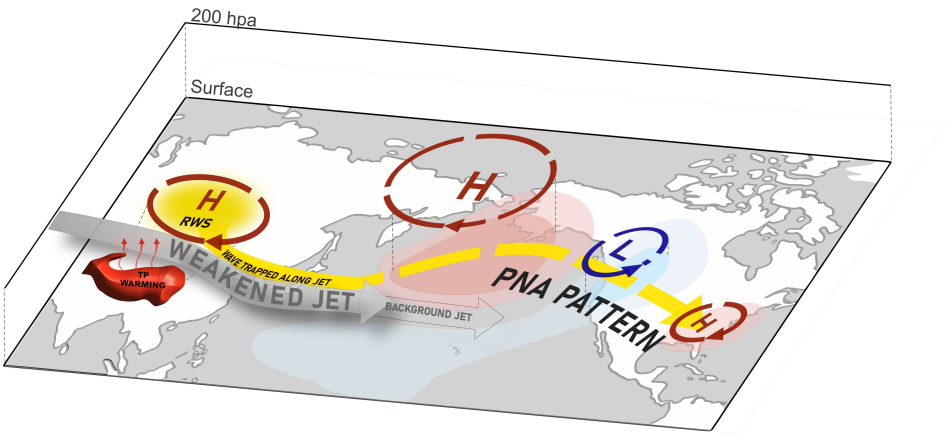


Fig. 5: Schematic of the proposed mechanism linking Tibetan Plateau (TP) warming to the negative Pacific–North American (PNA) pattern. Red shading over the Tibetan Plateau indicates imposed surface warming, with red arrows denoting anomalous ascent. The yellow ellipses and arrow display the Rossby Wave Source (RWS) and the resulting wave train respectively. The grey arrow shows the subtropical jet, with its control position outlined. Red and blue shading shows positive and negative geopotential height anomalies, labeled H and L respectively.

This mechanism is dynamically consistent and expands on previous TP cooling and PNA studies (Wang et al. 2020; Qian et al. 2019; Lin and Wu 2011; Seo and Lee 2017). Previous studies have primarily focused on snowfall anomalies as an important TP forcing mechanism, particularly through their influence on surface energy balance and diabatic heating. Earlier snowfall-based studies reported a weakening TP–PNA relationship in recent decades, attributed to a reduced cooling anomaly over the plateau (Qian et al. 2019; Wang et al. 2020). By isolating the thermal forcing response of the TP, without prescribing a snowfall anomaly, the present results demonstrate that TP warming can independently contribute to a negative PNA-like circulation response. These results highlight the importance of TP thermal forcing magnitude in modulating this teleconnection and suggest that future changes in the TP mean thermal state may play a larger role in North American winter variability than previously emphasized.

It is important to note that this investigation is based on a single model system and purposely excludes coupling with dynamic ocean processes, which can influence atmospheric circulation, most notably the ocean influence on the mid-latitude westerlies whose position is vital for the establishment of this teleconnection (Deser et al. 2015). A study from Liu et al. (2023) using a coupled atmospheric-oceanic general circulation model found that the ocean-atmosphere interaction amplified the TP-PNA response from snowfall anomalies. Likewise, Sun et al. (2019) found that ocean-atmosphere interactions can deepen anomalies over the North Pacific induced by surface heating over the TP in spring. Therefore, the atmospheric response identified in this study likely represents a lower bound of the full coupled response. Future work should investigate the sensitivity of this teleconnection to prescribed SST patterns versus fully coupled configurations.

At the same time, the future TP climate response remains uncertain and dynamically complex (Wang et al. 2025). Although mean temperatures over the TP are projected to increase substantially during the twenty-first century, episodic extreme snowfall events may still occur. In such cases, the combined influence of a warmer background state and snowfall anomalies must be considered, as both may contribute to the total atmospheric forcing. Understanding this balance will require improved representation of TP land–atmosphere interactions, snow–albedo feedbacks, and complex terrain processes in climate models. Such improvements will be important for constraining future projections of both TP warming and associated North American winter climate variability.

References

Bao, Q., Yang, J., Liu, Y., Wu, G., Wang, B.: Roles of anomalous tibetan plateau warming on the severe 2008 winter storm in central-southern china. Monthly Weather Review **138**(6), 2375–2384 (2010)

Deser, C., Tomas, R.A., Sun, L.: The role of ocean–atmosphere coupling in the zonal-mean atmospheric response to arctic sea ice loss. Journal of Climate **28**(6), 2168–2186 (2015) https://doi.org/10.1175/JCLI-D-14-00325.1

Hu, S., Hsu, P.-C., Li, W., Wang, L., Chen, H., Zhou, B.: Mechanisms of tibetan plateau warming amplification in recent decades and future projections. Journal of Climate **36**(17), 5775–5792 (2023) https://doi.org/10.1175/JCLI-D-22-0471.1

Hu, S., Wang, L., Chen, X., Zhou, T., Hsu, P.-C.: Emergent constraints on future projections of tibetan plateau warming in winter. Geophysical Research Letters **51**(9), 2024–108728 (2024) https://doi.org/10.1029/2024GL108728 https://agupubs.onlinelibrary.wiley.com/doi/pdf/10.1029/2024GL108728. e2024GL108728 2024GL108728

Huang, J., Zhou, X., Wu, G., Xu, X., Zhao, Q., Liu, Y., Duan, A., Xie, Y., Ma, Y., Zhao, P., Yang, S., Yang, K., Yang, H., Bian, J., Fu, Y., Ge, J., Liu, Y., Wu, Q., Yu, H., Wang, B., Bao, Q., Qie, K.: Global climate impacts of land-surface and atmospheric processes over the tibetan plateau. Reviews of Geophysics **61**(3), 2022–000771 (2023) https://doi.org/10.1029/2022RG000771 https://agupubs.onlinelibrary.wiley.com/doi/pdf/10.1029/2022RG000771. e2022RG000771 2022RG000771

Lin, H., Wu, Z.: Contribution of the autumn tibetan plateau snow cover to seasonal

prediction of north american winter temperature. Journal of Climate **24**(11), 2801–2813 (2011)

Lin, H., Wu, Z.: Contribution of tibetan plateau snow cover to the extreme winter conditions of 2009/10. Atmosphere-Ocean **50**(1), 86–94 (2012) https://doi.org/10.1080/07055900.2011.649036

Liu, S., Wu, Q., Ren, X., Yao, Y., Schroeder, S.R., Hu, H.: Modeled northern hemisphere autumn and winter climate responses to realistic tibetan plateau and mongolia snow anomalies. Journal of Climate **30**(23), 9435–9454 (2017)

Liu, S., Wu, Q., Schroeder, S.R., Yao, Y., Zhang, Y., Wu, T., Wang, L., Hu, H.: Near-global atmospheric responses to observed springtime tibetan plateau snow anomalies. Journal of Climate **33**(5), 1691–1706 (2020)

Liu, S., Wu, Q., Yao, Y., Schroeder, S.R.: The role of coupled north pacific atmosphere–ocean interactions in impacts of tibetan plateau snow anomalies on the northern hemisphere winter atmospheric circulation. Journal of Climate **36**(5), 1369–1385 (2023) https://doi.org/10.1175/JCLI-D-22-0261.1

Lu, M., Yang, S., Li, Z., He, S., Wang, Z.: Possible effect of the tibetan plateau on the "upstream" climate over west asia, north africa, south europe and the north atlantic. Climate Dynamics **51**, 1485–1498 (2018) https://doi.org/10.1007/s00382-017-3966-5

Meng, Y., Duan, K., Shi, P., Shang, W., Li, S., Cheng, Y., Xing, L., Chen, R., He, J.: Sensitive temperature changes on the tibetan plateau in response to global warming. Atmospheric Research **294**, 106948 (2023) https://doi.org/10.1016/j.atmosres.2023.106948

Meier, W., Fetterer, F., Windnagel, A., Stewart, J.S., Stafford, T.: Near-Real-Time

NOAA/NSIDC Climate Data Record of Passive Microwave Sea Ice Concentration, Version 3. National Snow and Ice Data Center (2024). https://doi.org/10.7265/J0Z0-4H87 . https://nsidc.org/data/g10016/versions/3

NOAA Climate Prediction Center: Monthly mean pna index. NOAA Climate Prediction Center (2005). Accessed: 2026-05-24

Plumb, R.A.: On the three-dimensional propagation of stationary waves. Journal of Atmospheric Sciences **42**(3), 217–229 (1985)

Qian, Q., Jia, X., Wu, R.: Changes in the impact of the autumn tibetan plateau snow cover on the winter temperature over north america in the mid-1990s. Journal of Geophysical Research: Atmospheres **124**(19), 10321–10343 (2019) https://doi.org/10.1029/2019JD030245 https://agupubs.onlinelibrary.wiley.com/doi/pdf/10.1029/2019JD030245

Seland, Ø., Bentsen, M., Olivié, D., Toniazzo, T., Gjermundsen, A., Graff, L.S., Debernard, J.B., Gupta, A.K., He, Y.-C., Kirkevåg, A., Schwinger, J., Tjiputra, J., Aas, K.S., Bethke, I., Fan, Y., Griesfeller, J., Grini, A., Guo, C., Ilicak, M., Karset, I.H.H., Landgren, O., Liakka, J., Moseid, K.O., Nummelin, A., Spensberger, C., Tang, H., Zhang, Z., Heinze, C., Iversen, T., Schulz, M.: Overview of the norwegian earth system model (noresm2) and key climate response of cmip6 deck, historical, and scenario simulations. Geoscientific Model Development **13**(12), 6165–6200 (2020) https://doi.org/10.5194/gmd-13-6165-2020

Sun, R., Duan, A., Chen, L., Li, Y., Xie, Z., Zhao, Y.: Interannual variability of the north pacific mixed layer associated with the spring tibetan plateau thermal forcing. Journal of Climate **32**(11), 3109–3130 (2019) https://doi.org/10.1175/JCLI-D-18-0577.1

Seo, K.-H., Lee, H.-J.: Mechanisms for a pna-like teleconnection pattern in response to the mjo. Journal of the Atmospheric Sciences **74**(6), 1767–1781 (2017) https://doi.org/10.1175/JAS-D-16-0343.1

Smith, D.M., Screen, J.A., Deser, C., Cohen, J., Fyfe, J.C., García-Serrano, J., Jung, T., Kattsov, V., Matei, D., Msadek, R., Peings, Y., Sigmond, M., Ukita, J., Yoon, J.-H., Zhang, X.: The Polar Amplification Model Intercomparison Project (PAMIP) contribution to CMIP6: Investigating the causes and consequences of polar amplification. Geoscientific Model Development **12**(3), 1139–1164 (2019) https://doi.org/10.5194/gmd-12-1139-2019

United Nations Environment Programme: A scientific assessment of the third pole environment. UNEP Scientific Assessment Series **1**(1), 1–180 (2022). UN Environment Document Repository

Wang, K., Chen, Q., Ge, F., Lin, Z.: Revisiting the future changes in precipitation extremes over the Eastern Tibetan Plateau: From the thermodynamic–dynamic processes to model uncertainty. Climate Dynamics **63**(3), 144 (2025) https://doi.org/10.1007/s00382-025-07620-z

Wu, Q., Hu, H., Zhang, L.: Observed influences of autumn–early winter eurasian snow cover anomalies on the hemispheric pna-like variability in winter. Journal of Climate **24**(7), 2017–2023 (2011)

Wang, Z., Wu, R., Duan, A., Qu, X.: Influence of eastern tibetan plateau spring snow cover on north american air temperature and its interdecadal change. Journal of Climate **33**(12), 5123–5139 (2020)

Zhou, M., Yu, Z., Gu, H., Wang, W.: Evaluation and projections of surface air temperature over the tibetan plateau from cmip6 and cmip5: warming trend

and uncertainty. Climate Dynamics **60**, 3863–3883 (2023) https://doi.org/10.1007/s00382-022-06518-4

Statements and Declarations

Acknowledgements. This research has been supported by the Research Council of Norway (grant nos. 328935) under the project COMBINED. We thank Sigma2 for the computing and storage resources (nn9039k and NS9039K).

Author contributions. FR and IB designed and conducted the experiments with support from LS. FR caried out analysis and wrote the paper and with contributions from IB, LS, and FL. All of the authors contributed to the final paper.

Competing Interests. The authors have no relevant financial or non-financial interests to disclose

Data Availability. ERA5 reanalysis data are available from the Copernicus Climate Data Store (https://doi.org/10.24381/cds.6860a573). NOAA/NSIDC sea-ice concentration data are available at https://doi.org/10.7265/J0Z0-4H87. NorESM2-MM model output from the CONTROL and WTP simulations, and the analysis code, are archived at [DOI].